"Charge Leakage" at $LaMnO_3/SrTiO_3$ Interfaces

By *Javier Garcia-Barriocanal, Flavio Y. Bruno, Alberto Rivera-Calzada, Zouhair Sefrioui, Norbert M. Nemes, Mar Garcia-Hernández, Juan Rubio-Zuazo, German R. Castro, Maria Varela, Stephen J. Pennycook, Carlos Leon,* and *Jacobo Santamaria**

Epitaxial interfaces between complex oxides are of increasing interest due to the possibility of tailoring their electronic structures to display novel behaviors and functionalities.[1–7] At the interface between band insulators $SrTiO_3$ (STO) and $LaAlO_3$ (LAO), the polar discontinuity drives a charge-transfer process that causes the interface to become metallic[1] and eventually also superconducting[2,3] or ferromagnetic.[4] Moreover, the carrier density of this metallic state can be electrostatically controlled.[5,6] In a very related context, the electronic reconstruction occurring at the interface between a Mott insulator and a band insulator is also a very-interesting phenomenon.[8–13] It has been shown that when members of the same ABO_3 perovskite series (same B-site element) with divalent (Sr) and trivalent (La) A-site elements are combined in a $SrTiO_3$ (STO)/$LaTiO_3$ (LTO) heterostructure, a metallic state appears at the interface.[8,9,11] Dynamical mean-field-theory studies have shown that this metallic state, with unexpected conducting and spin properties, is driven by the difference in electrochemical potential at the interface, which causes charges to "leak" into the empty conduction band of the divalent compound.[9]

An important question not addressed so far is whether charge leakage occurs at interfaces between Mott and band insulating perovskites of different series (with different B-site elements). This issue deserves special attention since charge leakage may directly influence the operation and performance of practical oxide electronic devices, such as magnetic tunnel junctions or field-effect transistors, whose operation is dictated by these interfaces. Moreover, strain-induced structural distortions, controlled by the difference in B-site elements, trigger modifications of the bonding at the interface, which may affect the charge-leakage phenomenon. Here, we examine charge leakage at the interface between two oxide materials with different B-site cations: $SrTiO_3$ (STO) and $LaMnO_3$ (LMO), which is of special relevance in practical spintronic devices. This system incorporates a polar discontinuity at the interface, as in LAO/STO, such that similarly interesting physics may play a role in these multilayers. Using combined atomic column resolution imaging and spectroscopy, we provide direct evidence for charge leakage. Due to the discontinuous BO_6 network, an unambiguous change of the Ti oxidation state from 4+ to 3+ at the interface is resolved, resulting from the transfer of electrons from the manganite into the titanate layer. Moreover, we show that the direction of the charge leakage across the STO/LMO interface can be modified and even reversed by changing the LMO/STO thickness ratio. When this ratio is high, the manganite is relaxed and doped with holes. However, at low ratios it is doped with electrons, and under epitaxial strain, which deeply modifies the magnetism and transport. This finding highlights the importance of relative layer thicknesses and/or epitaxial strain in controlling doping at the interface and may result in future avenues for the design of new device concepts.

We have grown epitaxial $(LMO_M/STO_N)_8$ superlattices, with M and N ranging from 3 to 17 and 2 to 12 unit cells, respectively, on STO (100) substrates. In (100)-oriented STO layers ($Sr^{+2}O$) atomic planes alternate with ($Ti^{+4}O_2$) planes, which defines an empty t_{2g} valence band of a band-insulating compound (the oxidation states here are understood as the number of electrons donated by the cation into the O 2p bands). On the other hand in the LMO perovskite with the trivalent A-site element, charged $(La^{+3}O)^+$ atomic planes alternate with $(Mn^{+3}O_2)^-$ planes to define a half-filled e_g conduction band with localized carriers by on-site Coulomb repulsion (Mott–Hubbard insulator). Notice that, in contrast to the LTO/STO case, there is a breakdown in the BO_6 network at the interface with polar (charge) and orbital discontinuities. We will show that the different orbital symmetries at the two sides of the interface (e_g vs t_{2g}) may be responsible for the sensitivity of the electronic structure to the relative layer thicknesses.

Figure 1a shows a typical high-angle (θ–2θ) pattern of the $(LMO_{17}/STO_2)_8$ superlattice. The large number of (narrow) superlattice satellite peaks provides evidence for the structural coherence and the excellent crystalline quality of the samples. Figure 1b displays a high-magnification Z-contrast scanning transmission electron microscopy (STEM) image of the same sample. The layers show perfect epitaxial properties and coherent growth, which is in agreement with the X-ray results. The X-ray reflectivity patterns were analyzed using SUPREX 9.0[14] software and consistently show very-limited interface disorder (3 Å) and negligible chemical interdiffusion (below 5%). The

[*] Prof. J. Santamaria, Dr. J. Garcia-Barriocanal, F. Y. Bruno, Dr. A. Rivera-Calzada, Dr. Z. Sefrioui, Dr. N. M. Nemes, Prof. C. Leon
GFMC. Dpto. Física Aplicada III
Universidad Complutense de Madrid
28040 Madrid (Spain)
E-mail: jacsan@fis.ucm.es
Dr. M. Garcia-Hernández
Instituto de Ciencia de Materiales de Madrid-CSIC
Cantoblanco E-28049 Madrid (Spain)
Dr. J. Garcia-Barriocanal, Dr. J. Rubio-Zuazo, Dr. G. R. Castro
SpLine Spanish CRG Beamline at the ESRF
Grenoble cedex ESRF, BP 220-38043 (France)
Dr. M. Varela, Dr. S. J. Pennycook
Materials Science and Technology Division
Oak Ridge National Laboratory
Oak Ridge, TN 37831, (USA)

DOI: 10.1002/adma.200902263

low-magnification image shown in the inset of Figure 1b reveals continuous and flat layers over long lateral distances. Electron-energy-loss spectroscopy (EELS) spectra were acquired to investigate the interface structure. Figure 1c shows a high-resolution image of a $(LMO_{17}/STO_{12})_8$ sample. The elemental maps corresponding to the Ti $L_{2,3}$, Mn $L_{2,3}$, La $M_{4,5}$ and, Sr $L_{2,3}$, edges are shown in Figure 1d–g, respectively. The atomic lattices of all of these elements are clearly resolved. The STEM specimens were relatively thick (many tens of nm) so the width of the interface (~1 nm) is dominated by beam broadening, not by delocalization of the inelastic interaction.[15] Interestingly, the LMO (STO) layer looks chemically wider in the La (Ti) image than in the Mn (Sr) map, as shown in the line-traces displayed in Figure 2d. The maps indicate a (TiO_2) atomic-plane termination for both the top and bottom interfaces of every STO layer. On the other hand, the LMO layers always start and terminate with a (LaO) plane. Hence, the interface structure found in these samples is always the same: a (LaO) plane from the manganite faces a (TiO_2) plane from the STO; that is to say, the stacking is: . . . – (TiO_2) – (SrO) – (TiO_2) – (LaO) – (MnO_2) – (LaO). . .. This

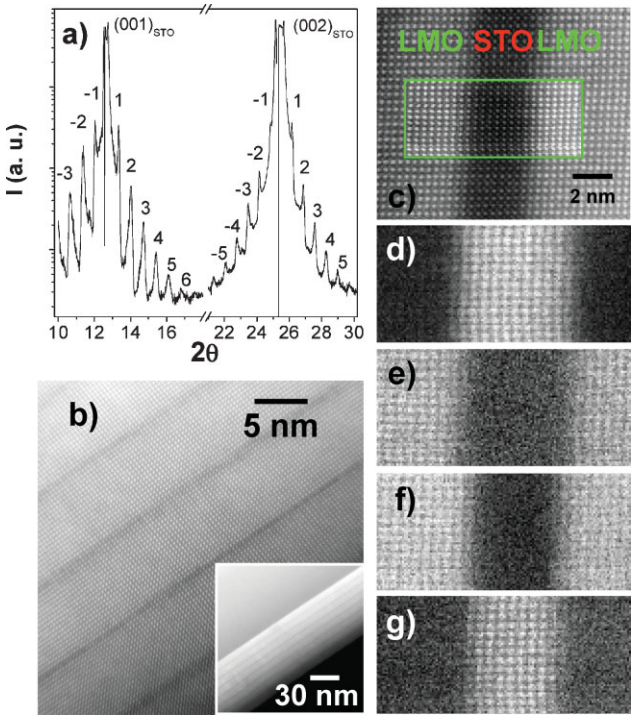

Figure 1. a) High-angle θ–2θ X-ray spectra of the $(LMO_{17}/STO_2)_8$ superlattice. The data was acquired with synchrotron radiation of wavelength 0.855 Å. The superlattice satellite peaks are indexed. b) High- and low- (inset) magnification *Z*-contrast images of the same sample, using a VG501 microscope. c) *Z*-contrast image of a $(LMO_{17}/STO_{12})_8$ superlattice. The green box marks the approximate region for electron-energy-loss-spectroscopy imaging. In the box, the annular dark field (ADF) signal acquired simultaneously with the spectrum image is shown. d–g) In black and white: atomic elemental maps obtained from the Ti $L_{2,3}$ (d), Mn $L_{2,3}$ (e), La $M_{4,5}$ (f) and Sr $L_{2,3}$, (g) edges (not to scale). The background was subtracted using a power-law fit. Windows of 30 eV were integrated under the edges. For the Sr $L_{2,3}$ edge a window of 200 eV was used. The data in the Figure 1c–g were obtained using the Nion UltraSTEM.

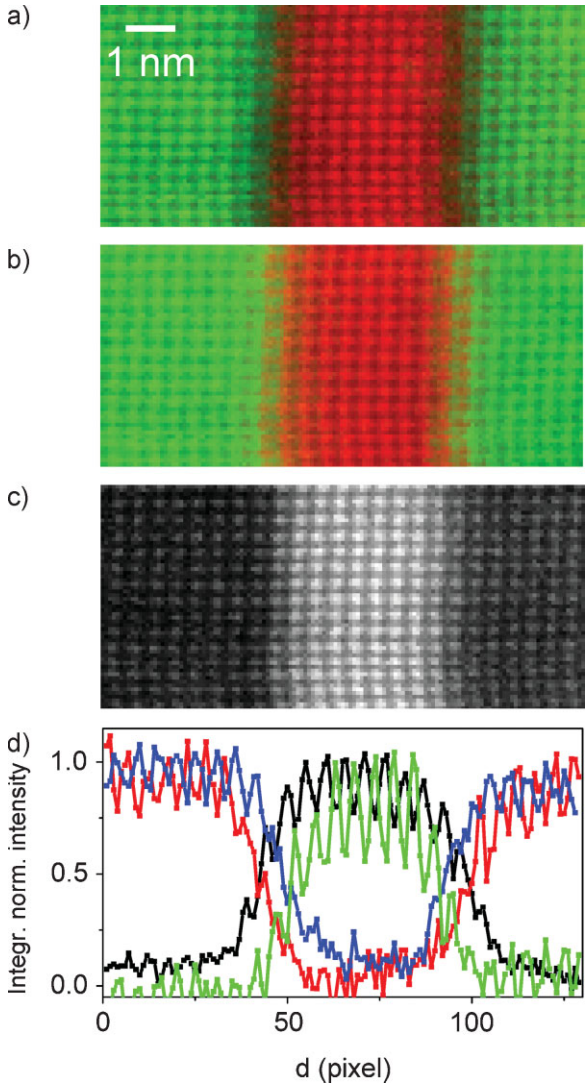

Figure 2. The color maps were produced by applying principal-component analysis to remove the noise from the EELS spectrum image and then overlaying the Sr image (red) and the Mn image (green) for Figure 2a, and the La image (green) and the Ti image (red) for Figure2b. c) Sr $L_{2,3}$ map obtained from the raw EELS spectrum image and subtracting the background using the spatial-difference technique [25]. For this purpose, a reference spectrum obtained through averaging of 800 spectra extracted from the middle of the LMO layers on both sides was used [26]. d) Normalized integrated intensities for the Ti $L_{2,3}$ (black), Mn $L_{2,3}$ (red), La $M_{4,5}$ (blue) and Sr $L_{2,3}$ (green), averaged along 10 vertical pixels across the elemental maps shown in Figure 1d–f and Figure 2c, respectively. The data were obtained using the Nion UltraSTEM.

stacking can be envisaged as a unit-cell-thick $LaTiO_3$ layer present at both interfaces. This fact becomes more evident when the images are superimposed. The color maps in Figure 2a–b show the elemental images discussed above, overlaid in pairs. Figure 2a is the superposition of the Sr map (red) and the Mn map (green), while Figure 2b shows the superposition of the Ti map (red) and the La image (green). While the interface regions in Figure 2a are basically dark, showing that no MnO_2 plane is in direct contact with a SrO plane, both interfaces in Figure 2b show that the LaO

and TiO_2 lattice images interpenetrate each other at the interfaces. Figure 2d shows the intensity traces of Ti, Mn, La and Sr across these images. All of the traces show a similar interfacial width of about three atomic planes, consistent with the expected beam broadening, but their relative offset clearly confirms the interface stacking sequence. This result is surprising since one would expect one of the interfaces to be terminated in (MnO_2) facing a (SrO) plane if the previous was terminated in (LaO) facing a (TiO_2) plane, but the EELS maps are unquestionable. The same interface structure was found in all of the samples in this study. The result implies that the interface structure we observe is the energetically preferred structure. Alternating interfacial structures may be expected on the basis of the surface energy, which is relevant during the growth process. However it is entirely reasonable that one specific interface structure will have the lowest interfacial energy, and, provided the growth process allows equilibrium to be achieved, then it will be observed at both interfaces. It is worth noting that we observe a similar symmetry in other perovskites-based superlattices obtained with the same growth system, such as $YBa_2Cu_3O_{7-x}/La_{0.7}Ca_{0.3}MnO_3$ (YBCO/LCMO).[16] In this case, both interface planes (top and bottom) show a ...CuO_2−BaO−MnO_2−La/CaO−... termination, with the CuO chains absent. In these samples, large CuO precipitates are occasionally observed over distances of micrometers,[17,18] which very likely act as a deposit for any excess material ensuing from the generation of symmetric interfaces.

One further aspect to be examined regards the in-plane structure, which is mostly determined by the epitaxial strain (approximately 1.1%). To probe the presence of structural distortions in the LMO/STO heterostructures we measured hkl reciprocal-space maps (RSMs) with synchrotron X-rays. Figure 3 displays the in plane RSM of the (103) direction of the LMO reciprocal space of the superlattices – (LMO_{17}/STO_2)$_8$ in Figure 3a and (LMO_7/STO_5)$_8$ in Figure 3b. Note that this reciprocal-space point of the LMO corresponds to the forbidden (0.5 0.5 1.5) reciprocal-space point of the STO and it is thus specific to the manganite. The superlattice with 2 unit cells of STO shows in-plane lattice parameters of $a = 3.95$ Å and $b = 3.865$ Å (Fig. 3a), consistent with a fully relaxed LMO phase.[19] However, when the STO thickness is increased up to 5 unit cells and the LMO thickness is reduced down to 7 unit cells (Fig. 3b), a perfectly epitaxial LMO phase is obtained with the bulk STO lattice parameters $a = b = 3.905$ Å. Samples with a large thickness ratio $t_r = t_{LMO}/t_{STO}$ have essentially relaxed LMO layers. Meanwhile, samples with small values of t_r show highly strained LMO layers and relaxed STO layers.

These changes in the thickness ratio have an important effect on the magnetic and transport properties. Hysteresis loops measured at 10 K and resistivity curves, displayed in Figure 4a and Figure 4b respectively, evidence ferromagnetism in the samples. It is worth mentioning that 22-unit-cell-thick LMO thin films showed ferromagnetic M(H) loops with a saturation magnetic moment of 2.2 μ_B/Mn at 10 K. The ferromagnetism is probably due to strain[20] or to cationic defects, which are known to hole-dope the LMO layers.[19] The average Mn oxidation-state values (measured close to 3+) set a relatively low limit to the density of defects in the single LMO layers. Surprisingly, the ferromagnetic fraction depends very strongly on the $t_r = t_{LMO}/t_{STO}$ layer-thickness ratio. The 1000 Oe field-cooling (FC) temperature-dependent magnetization (top inset of Fig. 4a) shows that the Curie temperature decreases with t_r, as does the saturation magnetization measured from the hysteresis loops in the main panel. Corresponding shifts are observed in the metal-insulator transition temperature (T_{MI}) in the resistivity curves displayed in Figure 4b. By reducing $t_r = t_{LMO}/t_{STO}$, the curves progressively change from metallic behavior (as observed in the (LMO_{17}/STO_2)$_8$ superlattice) to the

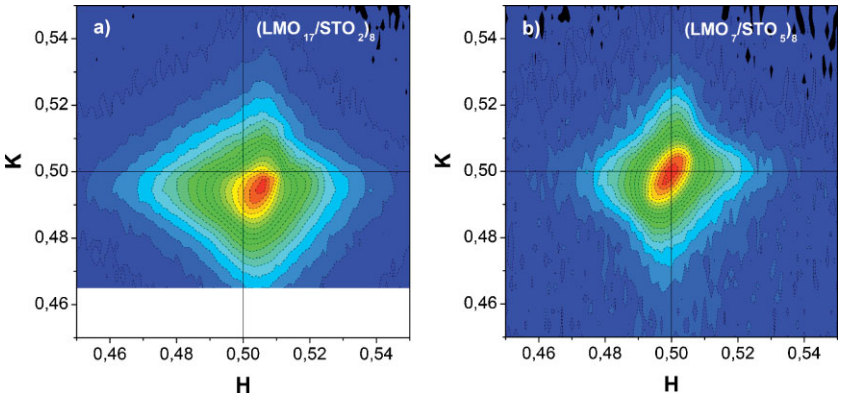

Figure 3. a) Reciprocal-space map (RSM) of the LMO layers of the (LMO_{17}/STO_2)$_8$ superlattice. b) RSM of the LMO layers of the (LMO_7/STO_5)$_8$ superlattice. The notation refers to the reciprocal-space units of the STO substrate.

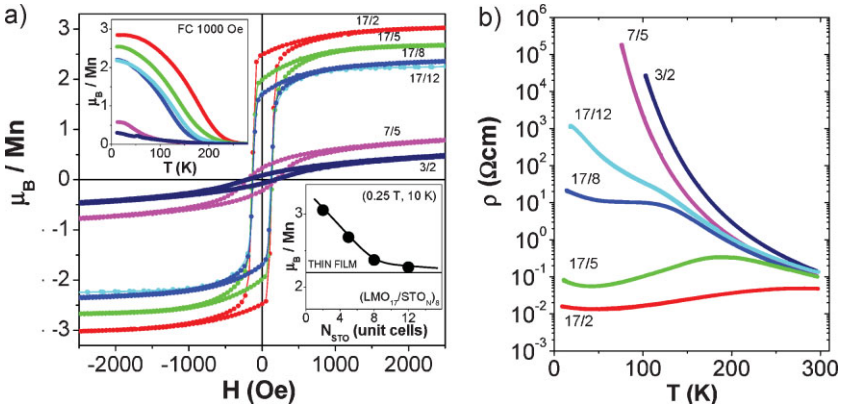

Figure 4. a) (SQUID) Hysteresis loops measured at 10 K. The N/M labels correspond to the LMO/STO layer thicknesses in unit cells. Top inset: FC magnetization versus temperature with an applied magnetic field of 1000 Oe. Bottom inset: Magnetization versus STO thickness of the (LMO_{17}/STO_n)$_8$ series measured at 10 K and 0.25 T. The line represents the magnetization of the 22-unit-cell LMO thin film measured under the same conditions. b) Logarithmic resistivity curves of the same samples. The same label nomenclature and color code has been used in both panels.

insulating behavior of the $((LMO_3/STO_2)_{30}$ superlattice. This points to the thickness ratio (and most likely, the ensuing degree of epitaxial strain) playing a determining role in the electronic properties of the system. It is also worth noting that these resistivity measurements rule out any major La/Sr interdiffusion in the system. The $(LMO_3/STO_2)_8$ sample is the most insulating of them all, and only weakly magnetic. Any significant La/Sr interdiffusion would cause the film to resemble the $La_{0.6}Sr_{0.4}MnO_3$ random alloy. However, this alloy is metallic and fully ferromagnetic, unlike what is shown by our data.

Such electronic properties can be studied in real space and with atomic resolution through the analysis of EELS spectra. EELS images such as the one in Figure 1 show that there is an additional (LaO) plane in every LMO layer. This extra $(La^{+3}O^{-2})$ plane has, on average, a donor character. Thus, its presence will have an influence on local layer doping. This doping can be examined through measurement of the transition metal oxidation states. For STO, the shape of the Ti $L_{2,3}$ edge (around 456 eV) depends on the filling of the titanium t_{2g} orbital.[21] As an example, Figure 5b shows the Ti L edge from bulk $SrTiO_3$ (Ti^{4+} (d^0)) (blue) and a thick $LaTiO_3$ film (Ti^{3+} (d^1)) (red), displaced vertically for clarity. We have utilized a method based on the spatial-difference technique[22] where the measured Ti $L_{2,3}$ edge is refined through a multiple linear least-squares fit (MLLS) to the reference data in Figure 5b. The MLLS fit coefficients through the EELS images represent the respective Ti^{3+}/Ti^{4+} weights, allowing spatial mapping of the Ti oxidation state.[8] Figure 5c and 5e display the results of the MLLS fits obtained for the $(LMO_{17}/STO_{12})_8$ and $(LMO_{17}/STO_2)_8$ superlattices, respectively, as a function of the distance (perpendicular) to the LMO/STO interface (top panels). STO ultrathin films of the $(LMO_{17}/STO_2)_8$ superlattices show mostly a Ti^{3+} oxidation state with a limited presence of the Ti^{4+} oxidation state, resulting from the proximity of both TiO_2 interfacial planes to LaO planes (i.e., both interfaces show a $LaTiO_3$ unit). However, the $(LMO_{17}/STO_2)_8$ superlattices show mostly a Ti^{3+} oxidation state. Since this result is most surprising, we also estimated the Ti oxidation state using a second independent method based on the analysis of the O K edge fine structure. The O K edge around 530 eV is also shown in Figure 5b, its fine structure also being different for both materials. The separation in energy between the pre-peak feature at the onset (marked with a vertical dashed line in Fig. 5b and the adjacent main peak (marked with vertical arrows), ΔE, decreases with nominal oxidation state in bulk STO and LTO. Assuming this decrease is linear, as in manganites,[23] and using the LTO and bulk STO ΔE as reference values, the Ti oxidation state can be extracted. Figure 5c and 5e show the values of ΔE across the $(LMO_{17}/STO_{12})_8$ and $(LMO_{17}/STO_2)_8$ superlattices, respectively (middle panels). The derived Ti oxidation state is plotted on the bottom panels (solid squares). This method gives almost-identical values for the Ti valence as the MLLS fit, confirming the overwhelming presence of Ti^{+3} in the strained $(LMO_{17}/STO_2)_8$ superlattice.[24] The presence of Ti^{3+} in the $(LMO_{17}/STO_2)_8$ superlattice, and the lack of it in the $(LMO_{17}/STO_{12})_8$ sample, evidences a "charge leakage" from the LMO layers into the STO: the additional (LaO) plane provides an extra electron, which electron-dopes the ultrathin (2 unit cells) STO layers. Since this "charge leakage" is not observed in the $(LMO_{17}/STO_{12})_8$ sample, which has the same interface atomic-plane stacking sequence, the process must be related to the changes promoted by the different thickness ratios in the samples. A thickness-modulated charge transfer also occurs in the LAO/STO system, where, above about 4 unit cells, charge will leak from the LAO valence band to the STO conduction band across the LAO film.[5] We cannot rule out that a similar process is occuring in our case. However, we would like to outline the important difference between both systems, that, in the case of a Mott insulator (LMO) in contact with a band insulator, there is already charge in the conduction band which may be transferred.

We next look for concomitant valence changes within the LMO layers, again focusing on the series of superlattices with constant LMO thickness (17 unit cells). The end members of this series are the $(LMO_{17}/STO_2)_8$ superlattice, showing electron leakage into the STO, and the $(LMO_{17}/STO_{12})_8$ superlattice, with mostly Ti^{4+} in the STO layers. The Mn^{4+}/Mn^{3+} ratio of our samples can also be determined, again from the ΔE parameter shown in Fig. 5b,

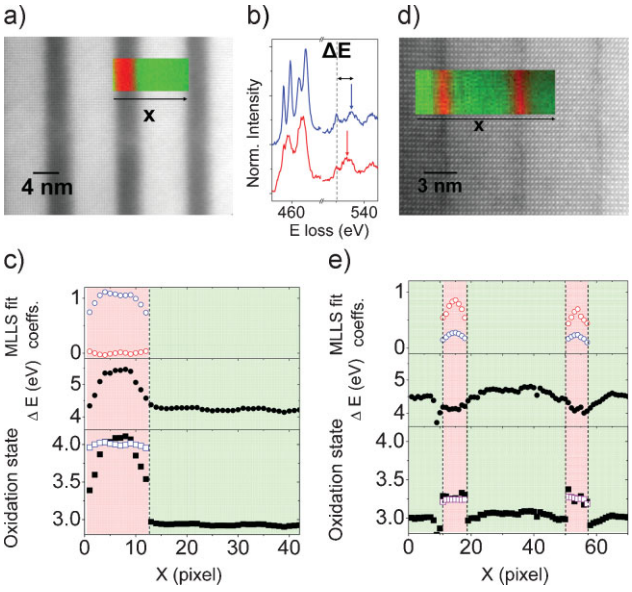

Figure 5. a) *Z*-contrast image of the $(LMO_{17}/STO_{12})_8$ superlattice. Inset: Color-coded chemical map for a STO/LMO bilayer in the same sample (to scale) – Ti signal in red and Mn in green (elemental Mn/Ti maps overlay as in Fig. 1d). b) EELS spectra showing the Ti $L_{2,3}$ and the O K edges for bulk STO (blue) and LTO (red). The spectra have been displaced vertically for clarity. The ΔE peak separation is marked. c) Mn and Ti oxidation states measured for the spectrum image shown in the inset to Figure 5a. The top panel shows the MLLS fit coefficients for the LTO spectrum (red) and the STO spectrum (blue). The middle panel shows the value of the ΔE parameter along the spectrum image. The bottom panel shows the transition metal oxidation state obtained from the MLLS fit (open squares) and from the ΔE parameter (solid squares). The background colors mark the approximate positions of the LMO (green) and the STO (red) layers. d) *Z*-contrast image of the $(LMO_{17}/STO_2)_8$ superlattice. Inset: Color-coded chemical map for an EELS spectrum image (to scale): Ti signal in red and Mn in green, superimposed as in Figure 5a. e) MLLS fit coefficients (top), ΔE parameter (middle), and transition metal oxidation states (bottom) for the $(LMO_{17}/STO_2)_8$ sample, same color code as in Figure 5c. All of the profiles have been obtained by averaging in the direction parallel to the interface across the whole spectrum image. STEM-EELS data in this figure were obtained in the VG501.

which in manganites shows a linear trend with oxidation state.[23] This analysis shows that the average Mn oxidation state is 3.05 ± 0.05 for the middle LMO layer of the $(LMO_{17}/STO_2)_8$ superlattice in Figure 5e and 2.93 ± 0.03 for the LMO layer of the $(LMO_{17}/STO_{12})_8$ sample in Figure 5c. Here, the error bars represent the standard deviation of the dataset. The reduced oxidation state in the relaxed $(LMO_{17}/STO_{12})_8$ sample is consistent with some degree of electron doping, most likely coming from the electron of the extra (LaO) plane. In fact, one extra electron evenly distributed among the 17 LMO unit cells would give rise to an average oxidation state of +2.94, in excellent agreement with the measured value. In summary, these changes suggest that the LMO layers are progressively more hole-doped when the STO thickness is reduced, which is consistent with an increased electron "leakage" into the STO. Further support for this picture comes from magnetotransport measurements. A gradual increase of the saturation magnetic moment is observed with decreasing STO thickness (see bottom inset of Fig. 4a), which correlates with both an increase of the Curie temperature and also a transition into a metallic state.

In summary, we have found a charge-leakage process at the manganite/titanate (LMO/STO) interfaces, controlled by relative thickness ratio. By modifying the STO spacer thickness we were able to control the doping (with electron or holes) of the manganite layers. Ultrathin STO layers yield hole-doped, relaxed manganite layers, while thicker STO layers result in strained manganite layers doped with electrons, evidencing a reversal of the sense of the charge leakage. This result highlights the important role played by the relative layer thickness in charge transfer at complex oxide interfaces. It is not possible to conclude from these experiments whether the effect is due to the change in thickness ratio, and hence electronic coupling between the two interfaces, or to the effect of epitaxial strain. These results should stimulate theoretical studies to gain more insight into the detailed mechanism. Furthermore, apart from its fundamental interest, it may also be important for the understanding of some reported limitations of oxide devices involving manganite/titanate interfaces and ultrathin (and thus strained) layers such as magnetic tunnel junctions and field-effect transistors.

Experimental

Samples were grown in a high-temperature (810 °C) sputtering apparatus [16–18,27,28]. X-ray reciprocal-space maps using a synchrotron radiation source (Spline beamline at the European Synchrotron Radiation Facility (ESRF)) providing a wavelength of 0.855 Å were measured in a six-circle diffractometer. The sample structure was also probed by scanning transmission electron microscopy (STEM). *Z*-contrast images were obtained using a VG Microscopes HB501UX instrument operated at 100 kV and equipped with a cold field-emission gun, a Nion aberration corrector and a Gatan Enfina electron-energy-loss spectrometer to allow simultaneous imaging and electron-energy-loss spectroscopy (EELS). Also, a Nion UltraSTEM operated at 100 kV and equipped with a 5th-order corrector and a Gatan Enfina EELS was used. Random noise in the EELS spectrum images was removed using principal-component analysis [29]. A two-contact, constant-current method with a guard electrode was used to measure the resistivity in the insulating samples, while the standard four-point-contact technique was used to measure the resistivity in the metallic samples.

Acknowledgements

The authors acknowledge Julia Luck for the preparation of the STEM specimen, Matt Chisholm for the LTO films and Masashi Watanabe for the Digital Micrograph plug-in for principal-component analysis. Research at ORNL (MV, SJP) was sponsored by the Division of Materials Sciences and Engineering of the US Department of Energy. We acknowledge the European Synchrotron Radiation Facility (ESRF) for provision of synchrotron radiation facilities. Research at UCM was supported by MICINN grant MAT2008 06517.

Received: July 7, 2009
Revised: July 24, 2009
Published online: November 24, 2009

[1] A. Ohtomo, H. Hwang, *Nature* **2004**, *427*, 423.
[2] N. Reyren, S. Thiel, A. D. Caviglia, L. Fitting Kourkoutis, G. Hammerl, C. Richter, C. W. Schneider, T. Kopp, A.-S. Rüetschi, D. Jaccard, M. Gabay, D. A. Muller, J.-M. Triscone, J. Mannhart, *Science* **2007**, *317*, 1196.
[3] A. D. Caviglia, S. Gariglio, N. Reyren, D. Jaccard, T. Schneider, M. Gabay, S. Thiel, G. Hammerl, J. Mannhart, J.-M. Triscone, *Nature* **2008**, *456*, 624.
[4] A. Brinkman, M. Huijben, M. van Zalk, J. Huijben, U. Zeitler, J. C. Maan, W. G. van der Wiel, G. Rijnders, D. H. A. Blank, H. Hilgenkamp, *Nat. Mater.* **2007**, *6*, 493.
[5] S. Thiel, G. Hammerl, A. Schmehl, C. W. Schneider, J. Mannhart, *Science* **2006**, *313*, 1942.
[6] C. Cen, S. Thiel, J. Mannhart, J. Levy, *Science* **2009**, *323*, 1026.
[7] J. Garcia-Barriocanal, A. Rivera-Calzada, M. Varela, Z. Sefrioui, E. Iborra, C. Leon, S. J. Pennycook, J. Santamaría, *Science* **2008**, *321*, 676.
[8] A. Ohtomo, D. A. Muller, J. L. Grazul, H. Hwang, *Nature* **2002**, *419*, 378.
[9] S. Okamoto, A. Millis, *Nature* **2004**, *428*, 630.
[10] M. Takizawa, H. Wadati, K. Tanaka, M. Hashimoto, T. Yoshida, A. Fujimori, A. Chikamatsu, H. Kumigashira, M. Oshima, K. Shibuya, T. Mihara, T. Ohnishi, M. Lippmaa, M. Kawasaki, H. Koinuma, S. Okamoto, A. J. Millis, *Phys. Rev. Lett.* **2006**, *97*, 057601.
[11] S. S. A. Seo, W. S. Choi, H. N. Lee, L. Yu, K. W. Kim, C. Bernhard, T. W. Noh, *Phys. Rev. Lett.* **2007**, *99*, 266801.
[12] Ş. Smadici, P. Abbamonte, A. Bhattacharya, X. Zhai, B. Jiang, A. Rusydi, J. N. Eckstein, S. D. Bader, J.-M. Zuo, *Phys. Rev. Lett.* **2007**, *99*, 196404.
[13] A. Bhattacharya, S. J. May, S. G. E. te Velthuis, M. Warusawithana, X. Zhai, Bin Jiang, J.-M. Zuo, M. R. Fitzsimmons, S. D. Bader, J. N. Eckstein, *Phys. Rev. Lett.* **2008**, *100*, 257203.
[14] a) I. K. Schuller, *Phys. Rev. Lett.* **1980**, *44*, 1597. b) W. Sevenhans, M. Gijs, Y. Bruynseraede, H. Homma, I. K. Schuller, *Phys. Rev. B: Condens. Matter* **1986**, *34*, 5955. c) E. E. Fullerton, I. K. Schuller, H. Vanderstraeten, Y. Bruynseraede, *Phys. Rev. B: Condens. Matter* **1992**, *45*, 9292. d) D. M. Kelly, E. E. Fullerton, J. Santamaria, I. K. Schuller, *Scr. Metall. Mater.* **1995**, *33*, 1603.
[15] M. P. Oxley, M. Varela, T. J. Pennycook, K. van Benthem, S. D. Findlay, A. J. D'Alfonso, L. J. Allen, S. J. Pennycook, *Phys. Rev. B: Condens. Matter* **2007**, *76*, 064303.
[16] M. Varela, A. R. Lupini, S. J. Pennycook, Z. Sefrioui, J. Santamaria, *Solid State Electron.* **2003**, *47*, 2245.
[17] M. Varela, Z. Sefrioui, D. Arias, M. A. Navacerrada, M. Lucía, M. A. López de la Torre, C. León, G. Loos, F. Sánchez-Quesada, J. Santamaría, *Phys. I Rev. Lett.* **1999**, *83*, 3936.
[18] M. Varela, W. Grogger, D. Arias, Z. Sefrioui, C. León, C. Ballesteros, K. M. Krishnan, J. Santamaría, *Phys. Rev. B: Condens. Matter* **2002**, *66*, 174514.

[19] a) J. Töpfer, J. B. Goodenough, *J. Solid State Chem.* **1997**, *130*, 117. b) J. M. D. Coey, M. Viret, *Adv. Phys.* **1999**, *48*, 167. c) C. Ritter, M. R. Ibarra, J. M. De Teresa, P. A. Algarabel, C. Marquina, J. Blasco, J. García, S. Oseroff, S. W. Cheong, *Phys. Rev. B: Condens. Matter* **1997**, *56*, 8902. d) R. Mahendiran, S. K. Tiwary, A. K. Raychaudhuri, T. V. Ramakrishnan, R. Mahesh, N. Rangavittal, C. N. R. Rao, *Phys. Rev. B: Condens. Matter* **1996**, *53*, 3348.

[20] C. Aruta, M. Angeloni, G. Balestrino, N. G. Boggio, P. G. Medaglia, A. Tebano, B. Davidson, M. Baldini, D. Di Castro, P. Postorino, P. Dore, *J. Appl. Phys.* **2006**, *100*, 023910.

[21] M. Abbate, F. M. F. de Groot, J. C. Fuggle, A. Fujimori, Y. Tokura, Y. Fujishima, O. Strebel, M. Domke, G. Kaindl, J. van Elp, B. T. Thole, G. A. Sawatzky, M. Sacchi, N. Tsuda, *Phys. Rev. B: Condens. Matter* **1991**, *44*, 5419.

[22] S. D. Berger, S. J. Pennycook, *Nature*, **1982**, *298*, 635.

[23] M. Varela, W. Luo, J. Tao, M. P. Oxley, M. Watanabe, A. R. Lupini, S. T. Pantelides, S. J. Penycook, *Phys. Rev. B: Condens. Matter* **2009**, *79*, 085117.

[24] The discrepancy between the two methods near the interfaces in the $(LMO_{17}/STO_{12})_8$ sample is most likely due to beam-broadening. The energy separation must change smoothly across the interface, since there is O on both sides. Therefore, the Ti oxidation state around +3.5 at the interface obtained by this method is an artifact due to averaging of both materials. On the other hand, the Ti edge fine structure does not, since there is no Ti in the LMO so the Ti oxidation-state value at the interface is accurately measured by this method. The reduced overall intensity is normalized out by the MLLS fitting procedure.

[25] M. Gao, C. Scheu, E. Tchernychova, M. Rühle, *J. Microsc.* **2003**, *210*, 94.

[26] Unfortunately, the Sr $L_{2,3}$ edge lies at very-high energy for EELS measurements, near 2000 eV. Therefore the Sr $L_{2,3}$ edges show a very-poor signal-to-noise ratio, hindering quantification efforts. To get more-reliable quantitative data we used two different background-subtraction methods: the power-law fit and the spatial-difference technique shown in Figure 2. The fact that a hint of atomic-resolution contrast is observed in the LMO side of the interface only for the second methods show that this is, most likely, an artifact.

[27] M. Varela, W. Grogger, D. Arias, Z. Sefrioui, C. León, C. Ballesteros, K. M. Krishnan, J. Santamaría, *Phys. Rev. Lett.* **2001**, *86*, 5156.

[28] Z. Sefrioui, D. Arias, V. Peña, J. E. Villegas, M. Varela, P. Prieto, C. León, J. L. Martinez, J. Santamaria, *Phys. Rev. B: Condens. Matter* **2003**, *67*, 214511.

[29] M. Bosman, M. Watanabe, D. T. L. Alexander, V. J. Keast, *Ultramicroscopy* **2006**, *106*, 1024.